Charge localization and reentrant superconductivity in a quasi-ballistic InAs nanowire coupled to superconductors

J. Estrada Saldaña, R. Žitko, J. Cleuziou, E. Lee, V. Zannier, D. Ercolani, L. Sorba, R. Aguado, S. de Franceschi

CONDENSED MATTER PHYSICS

Charge localization and reentrant superconductivity in a quasi-ballistic InAs nanowire coupled to superconductors

J. C. Estrada Saldaña[1]*, R. Žitko[2,3], J. P. Cleuziou[1], E. J. H. Lee[1†], V. Zannier[4], D. Ercolani[4], L. Sorba[4], R. Aguado[5], S. De Franceschi[1‡]

A semiconductor nanowire with strong spin-orbit coupling in proximity to a superconductor is predicted to display Majorana edge states emerging under a properly oriented magnetic field. The experimental investigation of these exotic states requires assessing the one-dimensional (1D) character of the nanowire and understanding the superconducting proximity effect in the presence of a magnetic field. Here, we explore the quasi-ballistic 1D transport regime of an InAs nanowire with Ta contacts. Fine-tuned by means of local gates, the observed plateaus of approximately quantized conductance hide the presence of a localized electron, giving rise to a lurking Coulomb blockade effect and Kondo physics. When Ta becomes superconducting, this local charge causes an unusual, reentrant magnetic field dependence of the supercurrent, which we ascribe to a 0 - π transition. Our results underline the relevant role of unintentional charge localization in the few-channel regime where helical subbands and Majorana quasi-particles are expected to arise.

INTRODUCTION

Nanowires (NWs) with strong spin-orbit coupling and induced superconductivity have the potential to realize topological superconductivity (*1*, *2*). Majorana modes emerge if the one-dimensional (1D) character of the NW is preserved over micrometer-scale lengths and the chemical potential is positioned within the helical gap opened by a properly oriented magnetic field B (*3*). The Rashba spin-orbit energy in InAs NWs is, at most, of the order of 100 μeV, as deduced from measurements of weak antilocalization (*4*). Given the modest size of the spin-orbit energy, the second condition implies that the 1D conduction mode supporting Majoranas should be only slightly filled. For this reason, it is important to explore the properties of semiconductor NWs at low subband filling in the presence of the superconducting proximity effect and a magnetic field. To this aim, we investigate InAs NWs coupled to tantalum-based superconducting contacts with a high in-plane critical field, $B_c \sim 1.8$ T.

Conductance quantization is the experimental paradigm of ballistic 1D transport (*5*). In semiconductor NWs, this phenomenon is better observed at large magnetic field (*6*), where backscattering is reduced and spin degeneracy is lifted, leading to conductance steps of e^2/h, where e is the electron charge and h is the Planck constant. Recently, conductance quantization was also observed at zero magnetic field, with steps of $2\ e^2/h$ due to twofold spin degeneracy (*7*–*10*). In this work, we make use of two independently tunable bottom gates to tailor the potential landscape in the NW channel (*10*). Proper tuning of the applied gate voltages results in the creation of a local point contact exhibiting approximately quantized conductance plateaus in the few-subband regime. We find that unintentional charge localization, while seemingly suppressed at high magnetic field, becomes apparent at low B in both normal and superconducting regimes. In the normal state, the spin of the localized charge is screened by Kondo correlations, which shape the linear and nonlinear conductance at the onset of the first plateau.

Owing to the large electron g factor in InAs and the relatively large B_c, we are also able to investigate the superconducting proximity effect coexisting with a strong spin polarization. We observe a nonmonotonic behavior of the critical current as a function of B that can be understood as a Zeeman-driven quantum phase transition from a spin singlet ground state, with 0-phase-shift Josephson coupling, to a spin-1/2 ground state, with π-phase-shift Josephson coupling. Upon increasing B, the supercurrent first vanishes at the 0 - π transition and then recovers once the Zeeman energy is large enough to stabilize the spin-1/2 ground state. This interpretation is confirmed by theoretical calculations based on an Anderson-type model coupled to superconducting leads with strong and gate-dependent tunnel couplings. A reentrant supercurrent due to the same mechanism is also observed in a second device exhibiting a clear quantum dot behavior and Kondo effect.

RESULTS

We performed standard two-terminal low-temperature conductance measurements on an InAs NW with Ta superconducting contacts (device 1), under an external magnetic field aligned parallel to the long axis of the wire, shown in Fig. 1A (data for different angles can be found in the Supplementary Materials). The profile of the conduction band was locally tuned by two gates underneath the wire (see inset of Fig. 1D).

To look for conductance quantization, the device was first characterized in the normal state at $B = 2.9$ T, which is well above B_c; the linear conductance, G, was measured as a function of voltages V_{G2} and V_{G3} on gates 2 and 3, respectively (Fig. 1B). All data are corrected for the series resistance of the measurement circuitry (51.37 kilohms), unless explicitly stated. Two conductance plateaus, around $0.9e^2/h$ and $1.8e^2/h$, can be identified, which are close to the ideal values for one and two 1D

[1]Université Grenoble Alpes, CEA, INAC-PHELIQS, 38000 Grenoble, France. [2]Jožef Stefan Institute, Jamova 39, Ljubljana, Slovenia. [3]Faculty of Mathematics and Physics, University of Ljubljana, Jadranska 19, Ljubljana, Slovenia. [4]NEST–Istituto Nanoscienze–CNR and Scuola Normale Superiore, Piazza S. Silvestro 12, 56127 Pisa, Italy. [5]Materials Science Factory, Instituto de Ciencia de Materiales de Madrid (ICMM), Consejo Superior de Investigaciones Científicas (CSIC), Sor Juana Inés de la Cruz 3, 28049 Madrid, Spain.
*Present address: Center for Quantum Devices, Niels Bohr Institute, University of Copenhagen, 2100 Copenhagen, Denmark.
†Present address: Condensed Matter Physics Center (IFIMAC), Universidad Autónoma de Madrid, 28049 Madrid, Spain.
‡Corresponding author. Email: silvano.defranceschi@cea.fr

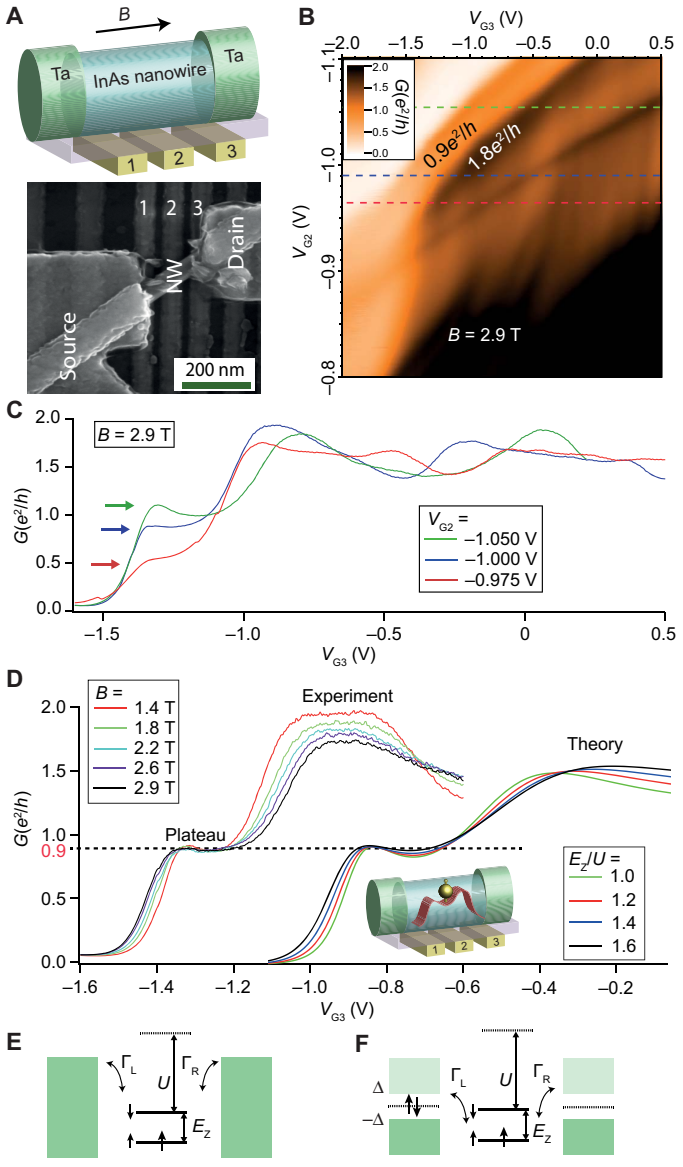

Fig. 1. Tuning of the conductance plateau of device 1 and quantum dot model. (**A**) Schematics and scanning electron micrograph of device 1. (**B**) Normal-state (B = 2.9 T) measurement of the linear conductance, G, as a function of V_{G2} and V_{G3} (in this color plot, black corresponds to $G > 2e^2/h$). Near pinch-off, two conductance plateaus appear at $G \approx 0.9e^2/h$ and $1.8e^2/h$. (**C**) $G(V_{G3})$ curves taken at V_{G2} = −0.975, −1, and − 1.05 V [dashed lines in (B)]. (**D**) Left: $G(V_{G3})$ curves measured at different B (V_{G2} = −1 V). The conductance of the $0.9e^2/h$ plateau remains unchanged within the explored B range. Right: NRG simulations of $G(V_{G3})$ at different values of the Zeeman energy, E_z, normalized to the charging energy U. The experimental and theoretical curves are shifted horizontally for clarity. Inset: Schematic representation of a camel-shape, conduction-band profile created by the local gates and the associated charge localization. (**E** and **F**) Representation of the single impurity Anderson model used to calculate (E) the normal-state conductance in (D), and (F) the Josephson current in Fig. 3 (E to H).

modes, i.e., e^2/h and $2e^2/h$, respectively. After a closer look, however, Fig. 1B shows noticeable structures consisting of conductance modulations of up to 20% superimposed on the quantized plateaus. We ascribe these modulations to tunneling resonances associated with quasi-localized states in the NW. These states are expected to have similar capacitive coupling to gates G2 and G3, hence producing the predominantly diagonal conductance ridges observed in Fig. 1B. The amplitude of these additional features varies over the (V_{G2},V_{G3}) plane and can vanish at certain regions.

Figure 1C shows three $G(V_{G3})$ traces taken at different V_{G2}. The green trace exhibits a clearly visible broad peak structure, causing an overshoot of the conductance at the onset of the first plateau. This structure is no longer present in the blue trace, resulting in an essentially flat conductance plateau. Further increasing V_{G2} results in a global suppression of the conductance step (red trace).

From now on, we focus on the intermediate value of V_{G2}, where the first conductance step shows no spurious resonances, thereby resembling the one expected for the onset of the first 1D conduction mode in a ballistic point contact. From a comparison with the other traces, we know that a resonance is lurking in this seemingly ideal plateau. This underlines the importance of double gate control in revealing the nature of the observed transport features. Furthermore, charge localization is apparent in the second plateau where conductance oscillations remain visible (Fig. 1C). The second plateau extends on a much larger V_{G3} range, suggesting that conductance is limited by the barrier induced by V_{G2}.

The first conductance plateau preserves its flat, featureless character over a large B range. Upon reducing B to 1.4 T (Fig. 1D), the plateau shrinks with B due to the decreasing Zeeman energy, $E_Z = |g| \mu_B B$, where μ_B is the Bohr magneton and g is the electron g factor in the point contact, while the conductance remains quantized at $0.9e^2/h$. The full-range B dependence is shown in Fig. 2A. At low B, the superconducting proximity effect causes the divergence of the conductance, simultaneously washing out the $0.9e^2/h$ plateau. This behavior can be seen from $G(V_{G3})$ traces below 1.4 T (Supplementary Materials) but hardly in Fig. 2A. Instead, Fig. 2A shows that, at large B, the $0.9e^2/h$ plateau widens linearly with B, as highlighted by two dashed lines. The two lines do not coalesce at $B = 0$ as expected, if the width of the plateau was simply proportional to E_Z. This zero-field splitting is again due to a localized charge state, most likely the same already identified at B = 2.9 T. The residual splitting is indicative of a sizable charging energy, U, associated with the localized state. We find $U \sim 1.3$ meV and $|g| = 11$ (Supplementary Materials). We convert V_{G3} scale into energy with the help of dI/dV measurements at finite source-drain bias voltage, V. This standard procedure (Supplementary Materials) yields a conversion factor of $\alpha = 0.0082$ meV/mV.

Localized states are often observed in semiconductor NWs. They can form (*11*–*13*) due to a plethora of confining mechanisms: crystal defects or impurities in the NW, tunnel barriers at the contacts, and surface charges. In a gate-defined point contact, where charge density is substantially lowered and electric field screening is consequently reduced, localization is enhanced and Coulomb interaction emerges. Strongly localized states leading to a few rather sharp Coulomb resonances can be observed in the studied gate-induced constriction near full charge depletion. They lie outside the (V_{G2}, V_{G3}) field explored in Fig. 1B (Supplementary Materials). The localized state at the onset of the first conductance plateau has a more subtle nature, and as we have seen, its presence may go unperceived without a proper control of the electrostatic landscape.

Before discussing the superconducting regime, it is instructive to examine the normal type behavior at $T > T_c$. Figure 2B shows $G(V_{G3})$ at 4.2 K. The onset of conduction through the first spin-degenerate subband is preceded by a shoulder at $\sim e^2/h$. A shoulder can also be consistently found in a measurement of dI/dV at 15 mK and $|eV| \gg \Delta$

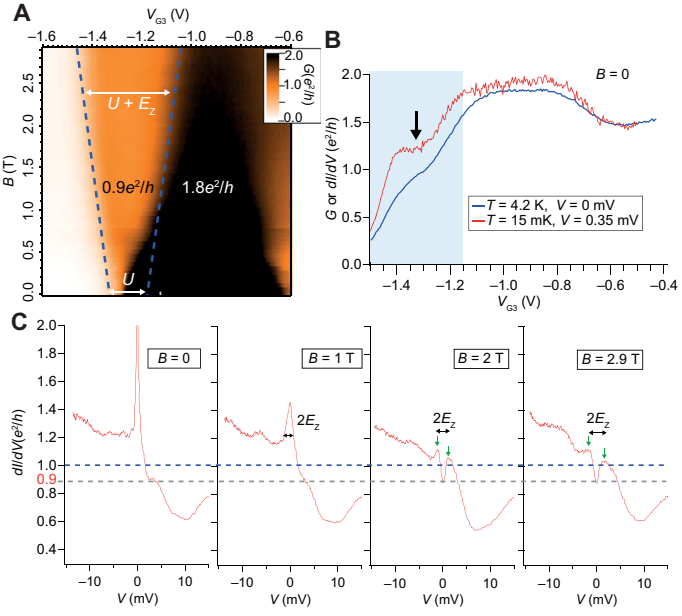

Fig. 2. Zeeman splitting of the plateau and associated Kondo feature. (**A**) Color plot of $G(B, V_{G3})$ (black corresponds to $G > 2e^2/h$) for device 1. The Zeeman-split conductance steps at higher B (onset marked by dashed lines) display a residual zero-field splitting set by U. (**B**) Zero B, normal-state conductance as a function of V_{G3}. $G(V_{G3})$ at 4.2 K, well above T_c (blue trace). Differential conductance, dI/dV, at 15 mK and $V = 0.35$ mV, i.e., well above the superconducting gap (red trace). Both curves display a shoulder at the position of the arrow. The blue-shaded region highlights the V_{G3} range in which the supercurrent regime is studied (Fig. 3). (**C**) $dI/dV(V)$ at different B ($T = 15$ mK) and fixed V_{G3} at the conductance shoulder. The split Kondo peaks are indicated by vertical green arrows. Their splitting is consistent with the simultaneously shown $2E_Z$ spacing calculated using $|g| = 11$.

(red trace). Here, $\Delta = 0.08$ meV is the induced superconducting gap measured by tunnel spectroscopy (Supplementary Materials).

This feature is reminiscent of a Kondo-screened bound state (*14*) as similarly observed in quantum point contacts (QPC) defined in a 2D electron gas (*15*). In that case, the conductance shoulder was identified with the 0.7 anomaly. The underlying Kondo physics is also apparent from $dI/dV(V)$ measurements for different B and fixed $V_{G3} = -1.25$ V at the conductance shoulder. The data (Fig. 2C) show the characteristic Zeeman splitting of a zero-bias Kondo resonance. At $B = 0$, the resonance has a zero-bias divergence due to the superconducting proximity effect. The Kondo effect gives rise to a characteristic logarithmic suppression of the conductance as a function of temperature. This aspect could be experimentally assessed but only after an accidental charge switching event, which changed the electrostatics of the device (Supplementary Materials).

To confirm our interpretation in terms of a quasi-ballistic QPC with a conductance anomaly arising from the screening of a localized spin-1/2 impurity, we model the device using the following Anderson-type Hamiltonian

$$H = \delta(n-1) + U/2(n-1)^2 + E_z S_z + \sum_{k\sigma}\varepsilon_k c^\dagger_{k\sigma}c_{k\sigma} + \sum_{k\sigma}\left(V^{(1)}(1-n_{d,\bar{\sigma}})c^\dagger_{k\sigma}d_\sigma + V^{(2)}n_{d,\bar{\sigma}}c^\dagger_{k\sigma}d_\sigma + \text{H.c.}\right) + \Delta\sum_k(c_{k\uparrow}c_{-k\downarrow} + \text{H.c.}) \quad (1)$$

Here, d_σ and $c_{k\sigma}$ are impurity and lead electron operators, respectively, where $\sigma \in \{\uparrow, \downarrow\}$ and k is the crystal momentum, $n = \Sigma_\sigma d^\dagger_\sigma d_\sigma$ is the localized level occupancy operator, δ is its energy position (later, we shall scale δ to V_{G3} for a direct comparison with the experimental data), and $S_z = (d^\dagger_\uparrow d_\uparrow - d^\dagger_\downarrow d_\downarrow)/2$ is the spin operator. The hybridization matrix elements for transitions between zero and one electrons, $V^{(1)}$, and one and two electrons, $V^{(2)}$, can be different (*14*). We parametrize this asymmetry through $x \equiv (V^{(1)} - V^{(2)})/V^{(1)}$, which is adjusted in our calculations to find the best agreement with the data. The coupling between the level and the leads results in a broadening $\Gamma = \pi |V^{(1)}|^2\rho$, where $\rho = \Sigma_k\delta(\omega - \varepsilon_k)$ is the density of states in the leads. Because the localized-state wavefunction depends on the (spin-dependent) trapping potential, we allow corrections to the hopping $V^{(1)}$, which are linear in δ (and hence V_{G3}) and B so that $\Gamma = \Gamma_0 + \Gamma_1(c_0 + c_1\delta/U + c_2E_Z/U)^2$. Physically, the B dependence can be expected from the influence of the magnetic field on the orbital motion and confinement of electrons. We introduced this broadening term to explicitly demonstrate, by comparing with the data, that the conductance through a correlated quantum dot can mimic plateaus of nearly quantized conductance. Our theory supports our physical interpretation. The parametrization for transport in the normal state qualitatively reproduces the experimental phenomenology in the superconducting state, as shown below. The last term in Eq. 1 accounts for superconducting pairing. The model was solved using the numerical renormalization group (NRG) method (*16, 17*). Above $\Gamma/U = 0.4$, charge quantization due to Coulomb blockade is lost, as determined from the charge susceptibility (Supplementary Materials). In the experiment, the first conductance plateau and the corresponding supercurrent data described below always occur for $\Gamma/U < 0.4$.

In the normal regime ($\Delta = 0$), the parameters are severely constrained even if only qualitative features of the conductance are to be reproduced for different T and B. At $B = 0$, Kondo correlations at finite T enhance the conductance to a value below the unitary limit producing a conductance shoulder at $\delta \sim 0$, as experimentally observed at $T = 4.2$ K (Fig. 2B). At finite B, the shoulder evolves into a plateau at $0.9e^2/h$. The results of the NRG calculations reproduce remarkably well the experimental trend, as shown in Fig. 1D. In particular, the calculated conductance at the spin-resolved plateau remains constant despite the large variation of E_z/U. The B-dependent term (proportional to c_2), even if small against the gate-dependent term (proportional to c_1), is essential. Without it, the plateau would evolve into a local minimum, as we actually find experimentally when B is applied perpendicularly to the NW under the same gate configuration (Supplementary Materials).

We now address the superconducting proximity effect. Figure 3 (A to D) shows supercurrent measurements as a function of V_{G3} at different values of B. Except for Fig. 3A, showing switching and retrapping currents directly measured at $B = 0$, the other panels display critical current, $j_c(V_{G3})$, traces obtained from fitting the measured $dI/dV(V)$ curves to the so-called resistively and capacitively shunted junction model (details on the measurement and fitting methodology are given in the Supplementary Materials). Fitting is necessary because increasing B makes the junction overdamped with a Josephson energy comparable to the thermal energy and no zero-resistance branch. While the normal conductance increases monotonically with V_{G3} [see the superimposed $G(V_{G3})$ trace in Fig. 3A], j_c does not, in contrast to the Ambegaokar-Baratoff relation, for which $j_c \sim G\Delta$. At $B = 0$, the switching currents (closely related to j_c) are slightly peaked in correspondence with the Kondo regime. Upon increasing B, $j_c(V_{G3})$ develops a minimum around $V_{G3} = -1.25$ V (Fig. 3B) and gets fully suppressed for $B = 0.75$ T (Fig. 3C) before reemerging at higher B (Fig. 3D).

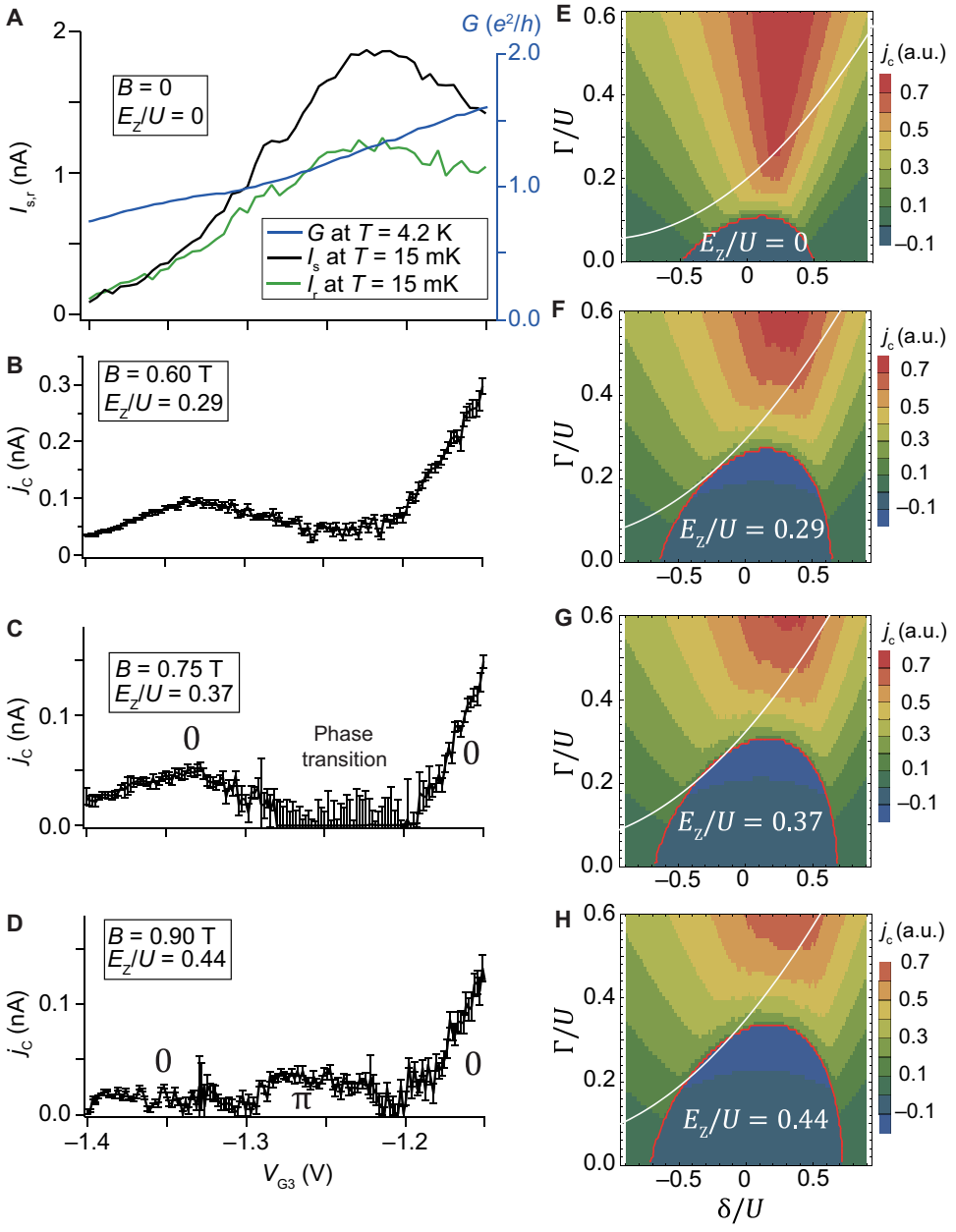

Fig. 3. Experimental supercurrent and corresponding quantum dot modeling. (**A** to **D**) Measured V_{G3} dependence of the switching currents I_r and I_s at $B = 0$ (A) and of the fitted critical current j_c at different B, hence E_Z/U (data from device 1). The normal-state G measured at 4.2 K and $B = 0$ is overlaid in (A). (**E** to **H**) NRG calculations of $j_c(\delta/U, \Gamma/U)$ for values of E_Z/U corresponding to the left panels. Each phase diagram has a closed region corresponding to a spin-1/2 ground state, surrounded by an open region where the ground state is a singlet. Crossing the boundary between these regions at constant superconducting phase difference results in a reversal of the supercurrent. To underline this effect, in the spin-1/2 region, we conventionally give a negative sign to j_c. The white lines represent the $\Gamma(\delta, E_Z)$ dependence obtained from the normal-state fit parameters. a.u., arbitrary units.

DISCUSSION

The behavior shown here can be explained using our model. The phase diagrams in Fig. 3 (E to H) show an open region where $j_c > 0$ (corresponding to a spin-singlet ground state) and a closed region where $j_c < 0$ (corresponding to a spin-1/2 ground state). The sign reversal reflects a π phase shift in the current-phase Josephson relation.

Because of correlated hopping ($x \neq 0$), the phase boundary has the shape of a skewed arc. At $B = 0$ (Fig. 3E), for odd charge ($-0.5 \lesssim \delta/U \lesssim 0.5$), strong (weak) coupling tends to stabilize a singlet (doublet) ground state (*18*–*25*). The singlet has a predominantly Bardeen-Cooper-Schrieffer character for $\Delta \gg \Gamma_S \gg U$ and a predominantly Kondo character for $\Gamma_S > \Delta$. The Zeeman effect is antagonistic to both of these many-body phenomena, thereby reducing the singlet binding energy and making the spin-1/2 domain grow with B (Fig. 3, F to H) (*26*), in agreement with the experiment (see additional j_c data in the Supplementary Materials).

These phase diagrams can account for the unusual, nonmonotonic B dependence of j_c observed experimentally. The white lines in Fig. 3

(E to H) denote the $\Gamma(\delta, E_Z)$ trajectory followed in the experimental sweeps, as deduced from normal-state fit parameters. As the doublet region of the phase diagram grows with E_Z, its phase boundary approaches the $\Gamma(\delta, E_Z)$ trajectory, leading to a suppression of j_c in the region of closest proximity. At $E_Z/U = 0.37$, the phase boundary reaches the $\Gamma(\delta, E_Z)$ trajectory, and j_c is correspondingly suppressed due to a competition between 0- and π-junction behavior. For larger E_Z, the $\Gamma(\delta, E_Z)$ trajectory crosses the spin-1/2 region, where the system acquires a clear π-junction behavior characterized by negative j_c.

Qualitatively, the observed gate dependence of I_c may also result from the opening of a helical gap due to Zeeman and spin-orbit interaction, as a gate voltage could potentially tune the chemical potential in and out of the helical gap in a hypothetical picture of noninteracting subbands (*27*). However, this interpretation is incompatible with our other observations in the same device.

In device 1, the charge localization responsible for the observed reentrant supercurrent was hidden by the seemingly ballistic transport. To further support the proposed physical picture, we performed a similar experimental study on a second device (device 2) displaying a quantum dot transport regime with clear Coulomb blockade oscillations. Device 2, shown in Fig. 4A, consists of an InAs NW contacted by superconducting Ta electrodes. Figure 4B shows a map of G as a function of back-gate voltage, V_{bg}, and side-gate voltage V_{sg}. We observe a Coulomb blockade pattern characteristic of single-dot transport with alternating large/small peak spacing, corresponding to even/odd occupation, respectively. We focus on the odd charge state indicated by a black arrow. The Coulomb peaks of this shell are renormalized by V_{sg}, a sign of Γ tuning.

Before describing the supercurrent behavior, we briefly characterize the normal-state regime by raising T above $T_c \approx 0.7$ K. Figure 4C shows a plot of the charge stability diagram taken at $V_{sg} = 1$ V, which exhibits the typical Coulomb diamonds of a high-impedance quantum dot. At odd filling (spin-1/2 ground state), we observe a zero-bias conductance ridge due to the Kondo effect. At finite magnetic field, the Kondo resonance splits due to Zeeman effect, as shown in Fig. 4D.

After corroborating the presence of the Kondo effect, we explored the B evolution of I_c at different V_{sg}. In Fig. 4E, we show fitted $I_c(V_{bg})$ curves obtained from one of these series of measurements at $V_{sg} = -1$ V. The curves display maxima in correspondence to the normal-state Coulomb peaks. As B is increased, these split apart due to Zeeman effect. Also, and more remarkably, a nonmonotonic behavior is observed in the Kondo valley, where I_c goes from 0.2 nA at $B = 0.2$ T to nearly zero at $B^* = 0.3$ T and then reenters at $B = 0.5$ T with a value of ≈ 0.1 nA. In our model, this is interpreted as a Zeeman-induced 0 → π transition from the destabilization of the Kondo singlet due to B-induced spin polarization. In Fig. 4F, we show the dependence of the crossover field at half-filling, B^*, on V_{sg}, as extracted from the B evolution of I_c at other V_{sg} values. As also predicted by our theory, lowering Γ (by increasing V_{sg}) reduces B^* all the way down to zero ($B^* = 0$ means that the junction is already at the π phase at $B = 0$).

We conclude that, even when seemingly absent, charge localization may play a crucial role in the transport properties of semiconductor NWs. In the superconducting regime, charge localization gives rise to a strong nonmonotonic behavior of the Josephson current as a function of B due to a Zeeman-induced 0 - π phase transition. Our findings are relevant to experiments aiming at detecting Majorana modes in Josephson junction geometries based on depleted NWs under strong Zeeman fields (*28*–*30*). The anomalous B-field dependence of the critical current, owing to the presence of Majoranas in the

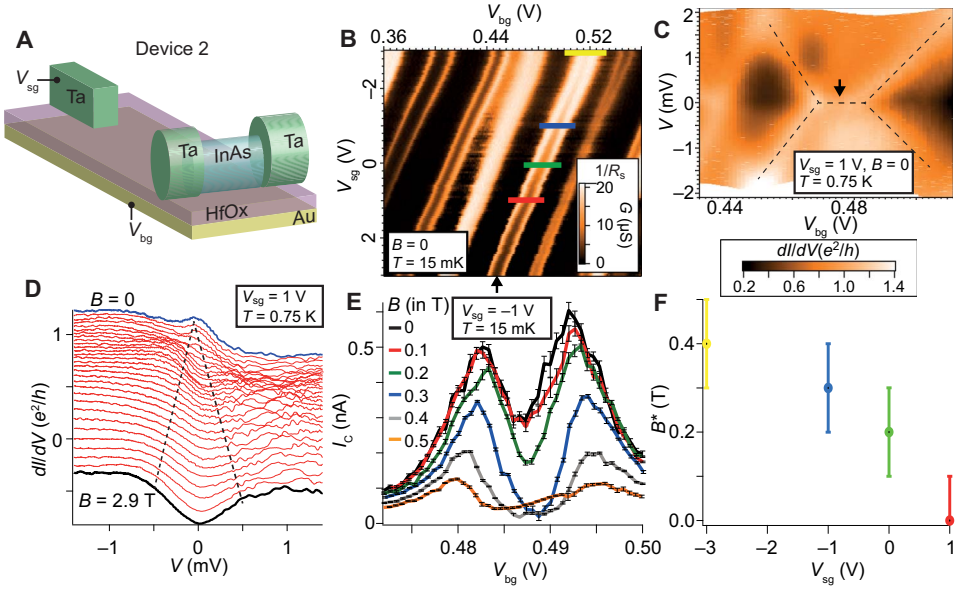

Fig. 4. Reproduction of reentrant supercurrent data in a closed quantum dot. (**A**) Schematics of device 2. (**B**) Color plot of $G(V_{bg}, V_{sg})$ for device 2. The data include the contribution of the series resistance ($R_S = 51.37$ kilohms) in the measurement circuit. White color corresponds to a nondissipative superconducting regime where $G = 1/R_S$. (**C**) Stability diagram, $dI/dV(V_{bg}, V)$, measured at the position of the red line in (B) at $T = 0.75$ K, i.e., just above T_c. A Kondo ridge at odd filling is indicated by an arrow. (**D**) Zeeman splitting of the Kondo resonance in the normal state taken in the middle of this Kondo ridge at 0.1-T increments. The traces are vertically shifted by $-0.025e^2/h$ for clarity. (**E**) B evolution of fitted $I_c(V_{bg})$ at the blue line in (B) and for different B (no offset). In the Kondo valley, I_c shows a reentrant behavior, vanishing at a crossover field $B^* \approx 0.3$ T and reemerging for $B > B^*$, heralding a ground-state transition from a Kondo singlet to a spin-split doublet. (**F**) Crossover field, B^*, versus V_{sg} as extracted from the B evolution of I_c at the corresponding linecuts in (B). The error bars are determined by the 0.1-T increment in B, as in (E).

junction (*31*–*33*), may be masked by the localization effects and the Kondo physics discussed here.

MATERIALS AND METHODS

Device 1, shown in Fig. 1A, was fabricated from a single 65-nm-diameter InAs NW grown by chemical beam epitaxy (*34*). The NW was deposited on a bed of narrow gate electrodes covered by 12 nm of HfO_2. Successively, Ta (60 nm)/Al (15 nm) source and drain contacts with a spacing of 280 nm were defined by electron-beam (e-beam) lithography and subsequent e-beam evaporation. The latter was preceded by a gentle in situ Ar etching to remove the native oxide of the NW. The Ta/Al contacts were measured to be superconducting below a critical temperature, $T_c \sim 0.8$ K, which is consistent with values reported for Ta in the crystalline β phase [$T_c = 0.67$ to 0.9 K (*35*)].

Device 2, shown in Fig. 4A, was fabricated from the same batch of InAs NWs as device 1. A 70-nm-diameter InAs NW was deposited on a single local back gate covered by 10 nm of HfO_2. Although the contacting procedure of the NW was similar to device 1, a Nb (5 nm)/Ta (80 nm) bilayer was used instead. The reasoning behind the inclusion of a thin Nb underlayer was the promotion of the high-T_c α phase; however, the convoluted superconducting gap was found to be as reduced as without Nb and $T_c = 0.7$ K. A side gate separated by 300 nm of vacuum was defined at the same moment as the contacts. B was applied at an 11° angle with respect to the long axis of the NW.

SUPPLEMENTARY MATERIALS

Supplementary material for this article is available at http://advances.sciencemag.org/cgi/content/full/5/7/eaav1235/DC1

Section S1. Lever-arm parameter
Section S2. Resonances before the conductance plateau
Section S3. Superconductivity-induced enhancement of the linear conductance below $B = 1.4$ T and residual $B = 0$ splitting
Section S4. Many-subband regime
Section S5. Dependence of the linear conductance on the magnetic field when aligned perpendicular to the axis of the NW
Section S6. Temperature dependence of a similar conductance shoulder
Section S7. Equivalent circuit and quality factor of the Josephson junction
Section S8. Method for fitting the supercurrent
Section S9. Evolution j_c near the 0–π transition
Section S10. Comparison between experimental and theoretical j_c
Section S11. Superconducting gap
Section S12. NRG calculations
Fig. S1. Lever-arm parameter calibration, demonstration of Γ tunability by the plunger gate, supercurrent enhancement of the linear conductance, and determination of U.
Fig. S2. Unconstrained conductance in a different gate setting.
Fig. S3. Absence of plateau for a magnetic field perpendicular to the NW.
Fig. S4. Normal-state measurements of a conductance shoulder similar to the one shown in the main text after an accidental gate shift.
Fig. S5. Measurement setup and fit example.
Fig. S6. Examples of raw supercurrent data and comparison to normal-state linear conductance.
Fig. S7. j_c extracted from fits to V-dI/dV curves taken at the same gate voltages and temperature as the data in Fig. 3 (A to D) but at different B field.
Fig. S8. Comparison between j_c linecuts (red line) taken at the white lines in Fig. 3 (E to H) and the experimental data from Fig. 3 (A to D) (black triangles or black line).
Fig. S9. Superconducting gap and its magnetic field dependence.
Fig. S10. Smearing of charge quantization with Γ.
References (*36*–*40*)

REFERENCES AND NOTES

1. R. M. Lutchyn, E. P. A. M. Bakkers, L. P. Kouwenhoven, P. Krogstrup, C. M. Marcus, Y. Oreg, Realizing Majorana zero modes in superconductor-semiconductor heterostructures. *Nat. Rev. Matter* **3**, 52–68 (2018).
2. R. Aguado, Majorana quasiparticles in condensed matter. *Riv. Nuovo Cimento* **40**, 523 (2017).
3. J. Chen, P. Yu, J. Stenger, M. Hocevar, D. Car, S. R. Plissard, E. P. A. M. Bakkers, T. D. Stanescu, S. M. Frolov, Experimental phase diagram of zero-bias conductance peaks in superconductor/semiconductor nanowire devices. *Sci. Adv.* **3**, e1701476 (2017).
4. Z. Scherübl, G. Fülöp, M. H. Madsen, J. Nygård, S. Csonka, Electrical tuning of Rashba spin-orbit interaction in multigated InAs nanowires. *Phys. Rev. B* **94**, 035444 (2016).
5. B. J. Van Wees, H. van Houten, C. W. J. Beenakker, J. G. Williamson, L. P. Kouwenhoven, D. van der Marel, C. T. Foxon, Quantized conductance of point contacts in a two-dimensional electron gas. *Phys. Rev. Lett.* **60**, 848–850 (1988).
6. I. V. Weperen, S. R. Plissard, E. P. A. M. Bakkers, S. M. Frolov, L. P. Kouwenhoven, Quantized conductance in an InSb nanowire. *Nano Lett.* **13**, 387–391 (2013).
7. S. Heedt, W. Prost, J. Schubert, D. Grützmacher, T. Schäpers, Ballistic transport and exchange interaction in InAs nanowire quantum point contacts. *Nano Lett.* **16**, 3116–3123 (2016).
8. J. Kammhuber, M. C. Cassidy, H. Zhang, Ö. Gül, F. Pei, M. W. A. de Moor, B. Nijholt, K. Watanabe, T. Taniguchi, D. Car, S. R. Plissard, E. P. A. M. Bakkers, L. P. Kouwenhoven, Conductance quantization at zero magnetic field in InSb nanowires. *Nano Lett.* **16**, 3482–3486 (2016).
9. H. Zhang, Ö. Gül, S. Conesa-Boj, M. P. Nowak, M. Wimmer, K. Zuo, V. Mourik, F. K. de Vries, J. van Veen, M. W. A. de Moor, J. D. S. Bommer, D. J. van Woerkom, D. Car, S. R. Plissard, E. P. A. M. Bakkers, M. Quintero-Pérez, M. C. Cassidy, S. Koelling, S. Goswami, K. Watanabe, T. Taniguchi, L. P. Kouwenhoven, Ballistic superconductivity in semiconductor nanowires. *Nat. Commun.* **8**, 16025 (2017).
10. J. C. Estrada Saldaña, Y.-M. Niquet, J.-P. Cleuziou, E. J. H. Lee, D. Car, S. R. Plissard, E. P. A. M. Bakkers, S. De Franceschi, Split-channel ballistic transport in an InSb nanowire. *Nano Lett.* **18**, 2282–2287 (2018).
11. K. Weis, S. Wirths, A. Winden, K. Sladek, H. Hardtdegen, H. Lüth, D. Grützmacher, T. Schäpers, Quantum dots in InAs nanowires induced by surface potential fluctuations. *Nanotechnology* **25**, 135203 (2014).
12. M. D. Schroer, J. R. Petta, Correlating the nanostructure and electronic properties of InAs nanowires. *Nano Lett.* **10**, 1618–1622 (2010).
13. B. Voisin, V.-H. Nguyen, J. Renard, X. Jehl, S. Barraud, F. Triozon, M. Vinet, I. Duchemin, Y.-M. Niquet, S. de Franceschi, M. Sanquer, Few-electron edge-state quantum dots in a silicon nanowire field-effect transistor. *Nano Lett.* **14**, 2094–2098 (2014).
14. Y. Meir, K. Hirose, N. S. Wingreen, Kondo model for the "0.7 anomaly" in transport through a quantum point contact. *Phys. Rev. Lett.* **89**, 196802 (2002).
15. S. M. Cronenwett, H. J. Lynch, D. Goldhaber-Gordon, L. P. Kouwenhoven, C. M. Marcus, K. Hirose, N. S. Wingreen, V. Umansky, Low-temperature fate of the 0.7 structure in a point contact: A kondo-like correlated state in an open system. *Phys. Rev. Lett.* **88**, 226805 (2002).
16. K. G. Wilson, The renormalization group: Critical phenomena and the Kondo problem. *Rev. Mod. Phys.* **47**, 773–840 (1975).
17. R. Bulla, T. A. Costi, T. Pruschke, Numerical renormalization group method for quantum impurity systems. *Rev. Mod. Phys.* **80**, 395–450 (2008).
18. T. Meng, S. Florens, P. Simon, Self-consistent description of Andreev bound states in Josephson quantum dot devices. *Phys. Rev. Lett.* **79**, 38–41 (2009).
19. J.-P. Cleuziou, W. Wernsdorfer, V. Bouchiat, T. Ondarçuhu, M. Monthioux, Carbon nanotube superconducting quantum interference device. *Nat. Nanotechnol.* **1**, 53–59 (2006).
20. J. A. Van Dam, Y. V. Nazarov, E. P. Bakkers, S. De Franceschi, L. P. Kouwenhoven, Supercurrent reversal in quantum dots. *Nature* **442**, 667–670 (2006).
21. H. I. Jørgensen, T. Novotný, K. Grove-Rasmussen, K. Flensberg, P. E. Lindelof, Critical current 0- transition in designed josephson quantum dot junctions. *Nano Lett.* **7**, 2441–2445 (2007).
22. A. Eichler, R. Deblock, M. Weiss, C. Karrasch, V. Meden, C. Schönenberger, H. Bouchiat, Tuning the Josephson current in carbon nanotubes with the Kondo effect. *Phys. Rev. B* **79**, 161407 (2009).
23. R. Maurand, T. Meng, E. Bonet, S. Florens, L. Marty, W. Wernsdorfer, First-order 0-π quantum phase transition in the kondo regime of a superconducting carbon-nanotube quantum dot. *Phys. Rev. X* **2**, 011009 (2012).
24. R. Delagrange, R. Weil, A. Kasumov, M. Ferrier, H. Bouchiat, R. Deblock, 0-π quantum transition in a carbon nanotube Josephson junction: Universal phase dependence and orbital degeneracy. *Phys. Rev. B* **93**, 195437 (2016).
25. E. J. H. Lee, X. Jiang, R. Žitko, R. Aguado, C. M. Lieber, S. De Franceschi, Scaling of subgap excitations in a superconductor-semiconductor nanowire quantum dot. *Phys. Rev. B* **95**, 180502 (2017).
26. E. J. H. Lee, X. Jiang, M. Houzet, R. Aguado, C. M. Lieber, S. De Franceschi, Spin-resolved Andreev levels and parity crossings in hybrid superconductor-semiconductor nanostructures. *Nat. Nanotechnol.* **9**, 79–84 (2014).

27. M. Cheng, R. M. Lutchyn, Josephson current through a superconductor/semiconductor-nanowire/superconductor junction: Effects of strong spinorbit coupling and Zeeman splitting. *Phys. Rev. B* **86**, 134522 (2012).
28. J. Tiira, E. Strambini, M. Amado, S. Roddaro, P. San-Jose, R. Aguado, F. S. Bergeret, D. Ercolani, L. Sorba, F. Giazotto, Magnetically-driven colossal supercurrent enhancement in InAs nanowire Josephson junctions. *Nat. Commun.* **8**, 14984 (2017).
29. K. Gharavi, G. W. Holloway, R. R. LaPierre, J. Baugh, Nb/InAs nanowire proximity junctions from Josephson to quantum dot regimes. *Nanotechnology* **28**, 085202 (2017).
30. K. Zuo, V. Mourik, D. B. Szombati, B. Nijholt, D. J. van Woerkom, A. Geresdi, J. Chen, V. P. Ostroukh, A. R. Akhmerov, S. R. Plissard, D. Car, E. P. A. M. Bakkers, D. I. Pikulin, L. P. Kouwenhoven, S. M. Frolov, Supercurrent interference in few-mode nanowire Josephson junctions. *Phys. Rev. Lett.* **119**, 187704 (2017).
31. P. San-Jose, E. Prada, R. Aguado, Mapping the topological phase diagram of multiband semiconductors with supercurrents. *Phys. Rev. Lett.* **112**, 137001 (2014).
32. J. Cayao, P. San-Jose, A. M. Black-Schaffer, R. Aguado, E. Prada, Majorana splitting from critical currents in Josephson junctions. *Phys. Rev. B* **96**, 205425 (2017).
33. P. San-Jose, J. Cayao, E. Prada, R. Aguado, Multiple Andreev reflection and critical current in topological superconducting nanowire junctions. *New J. Phys.* **15**, 075019 (2013).
34. U. P. Gomes, D. Ercolani, V. Zannier, F. Beltram, L. Sorba, Controlling the diameter distribution and density of InAs nanowires grown by Au-assisted methods. *Semicond. Sci. Technol.* **30**, 115012 (2015).
35. N. Schwartz, W. Reed, P. Polash, M. H. Read, Temperature coefficient of resistance of beta-tantalum films and mixtures with b.c.c.-tantalum. *Thin Solid Films* **14**, 333–346 (1972).
36. Y. M. Ivanchenko, L. A. Zil'berman, The Josephson effect in small tunnel contacts. *Sov. Phys. JETP* **28**, 1272 (1969).
37. V. Ambegaokar, B. I. Halperin, Voltage due to thermal noise in the dc Josephson effect. *Phys. Rev. Lett.* **23**, 1364–1366 (1969).
38. A. Steinbach, P. Joyez, A. Cottet, D. Esteve, M. H. Devoret, M. E. Huber, J. M. Martinis, Direct measurement of the Josephson supercurrent in an ultrasmall Josephson junction. *Phys. Rev. Lett.* **87**, 137003 (2001).
39. J. C. Estrada Saldaña, A. Vekris, G. Steffensen, R. Žitko, P. Krogstrup, J. Paaske, K. Grove-Rasmussen, J. Nygård, Supercurrent in a double quantum dot. *Phys. Rev. Lett.* **121**, 257701 (2018).
40. S. De Franceschi, L. Kouwenhoven, C. Schönenberger, W. Wernsdorfer, Hybrid superconductor–quantum dot devices. *Nat. Nanotechnol.* **5**, 703–711 (2010).

Acknowledgments

Funding: We acknowledge financial support from the Agence Nationale de la Recherche (TOPONANO project) and from the EU (ERC grant no. 280043). R.A. acknowledges financial support from the Spanish Ministry of Economy and Competitiveness (grant FIS2015-64654-P). R.Ž. acknowledges support from the Slovenian Research Agency (ARRS) under Program P1-0044 and J1-7259. **Author contributions:** V.Z., D.E., and L.S. grew the InAs NWs. R.Ž. and R.A. did the theoretical analysis. J.C.E.S. and J.P.C. fabricated the devices. J.C.E.S. performed the measurements. J.C.E.S., R.Ž., E.J.H.L., R.A., and S.D.F. analyzed the data, interpreted the results, and wrote the manuscript. **Competing interests:** The authors declare that they have no competing interests. **Data and materials availability:** All data needed to evaluate the conclusions in the paper are present in the paper and/or the Supplementary Materials. Additional data related to this paper may be requested from the authors.

Submitted 16 August 2018
Accepted 29 May 2019
Published 5 July 2019
10.1126/sciadv.aav1235

Citation: J. C. Estrada Saldaña, R. Žitko, J. P. Cleuziou, E. J. H. Lee, V. Zannier, D. Ercolani, L. Sorba, R. Aguado, S. De Franceschi, Charge localization and reentrant superconductivity in a quasi-ballistic InAs nanowire coupled to superconductors. *Sci. Adv.* **5**, eaav1235 (2019).

ScienceAdvances

Charge localization and reentrant superconductivity in a quasi-ballistic InAs nanowire coupled to superconductors

J. C. Estrada SaldañaR. ŽitkoJ. P. CleuziouE. J. H. LeeV. ZannierD. ErcolaniL. SorbaR. AguadoS. De Franceschi

Sci. Adv., 5 (7), eaav1235. • DOI: 10.1126/sciadv.aav1235

Science Advances (ISSN 2375-2548) is published by the American Association for the Advancement of Science. 1200 New York Avenue NW, Washington, DC 20005. The title *Science Advances* is a registered trademark of AAAS.